Indonesian Journal of Aerospace Vol. 23 No. 1 Juni 2025 : pp 77 – 96 (Bura et al.)
DOI: 10.59981/ijoa.2025.12201
https://ejournal.brin.go.id/ijoa/

Numerical Investigation of Supersonic and Hypersonic Shock-Wave/Boundary-Layer Interactions

Romie Oktovianus Bura[1], Graham T. Roberts[2], Yufeng Yao[3], Neil D. Sandham[4]

[1]Faculty of Defense Engineering and Technology, Republic of Indonesia Defense University (RIDU), Indonesia
[2,4]Aerodynamics & Flight Mechanics Research Group, University of Southampton, United Kingdom
[3]School of Engineering, University of West England, United Kingdom
e-mail: romiebura@idu.ac.id

Received:30-06-2025 Accepted: 27-08-2025. Published: 05-10-2025

Abstract

Numerical simulations of 2-D supersonic and hypersonic laminar Shock-Wave/ Boundary-Layer Interactions (SBLIs) were carried out by solving the Navier-Stokes (NS) equations using a compressible flow code over a wide range of Mach numbers and shock strengths. The results obtained at Mach 2.0 and 7.73 were compared with experimental data. In addition, the numerical data were further analyzed using correlation laws derived by previous researchers based on the free interaction concept, extended here to higher Mach numbers. The results indicate that this concept is valid for separated laminar hypersonic flows with SBLIs. For interference heating, the correlation technique based on the well-established power law relationship between peak heating and peak pressures yielded encouraging results consistent with other correlations for laminar interference heating at hypersonic speeds.

Keywords**:** *supersonic, hypersonic, shock-wave/ boundary-layer interactions, numerical*

1. Introduction

The interaction of shock-waves with developing boundary-layer flows occurs in many practical situations at transonic, supersonic, and hypersonic speeds. Often, the interaction results in boundary-layer separation with downstream reattachment. As a result, significant changes occur in the aerodynamic and thermal loads when the shock is strong. Shock-Wave/Boundary-Layer Interactions (SBLIs) are of special importance in hypersonic flows, since they can result in extremely high local heat-fluxes. Regions of particular concern are at wing-body or fin-body junctions, on deflected control surfaces (e.g., compression ramps), and near intakes on vehicles employing airbreathing propulsion. This problem is critical for the correct sizing of thermal protection systems (TPS) in parts of the vehicle where such interactions are likely to occur (Delery, 1999).

Due to the complexity of the phenomena involved, elucidating the flow physics and accurately estimating the pressure and heating levels generated in such interaction regions are extremely difficult. Consequently, TPS designs are typically conservative. This inevitably results in over-protection, leading to reduced payload capacity, reduced performance, higher costs, and possibly even reduced reliability (Holden, 1986). Thus, it remains an important goal to fully understand the flow phenomena associated with SBLIs.

In this study, results are presented from a numerical investigation of the impingement of an oblique shock-wave with a steady 2-D laminar boundary-layer growing over a flat plate. As the flow configuration involves shock-waves and flow separations, two of the most difficult features to reproduce numerically, it has become an important benchmark for validating new numerical methods. Additionally, due to its laminar character, it carries no flow uncertainty associated with turbulence modeling that may influence the solution. Although in most practical supersonic flow conditions the boundary-layer ahead of the SBLI is turbulent, for hypersonic flows at high altitudes, fully laminar and transitional (laminar-turbulent) interactions can exist in continuum flow.

This work aims to extend and validate correlation laws that predict the pressure rise and separation bubble length in 2-D SBLIs, as well as the prediction of peak heating within the interaction region, particularly in hypersonic flows. It is crucial to evaluate these flow parameters and assess their practical consequences early in the vehicle conceptual design phase, which is why such correlations can be highly useful.

This study is also a precursor to 3-D, unsteady simulations of a SBLI flow field in which perturbations are introduced to determine the boundary-layer stability and its propensity to undergo transition. The motivation for this latter work is to assess whether shock-induced transition in the separated shear layer of a SBLI flow field is responsible for the anomalously high heat-fluxes reported by Smith (1993) in compression-ramp experiments performed at the University of Southampton. Similar anomalously high heat-fluxes in laminar 2-D hypersonic flows with separation have also been reported by other researchers (Delery, 1996).

2. Methodology

2.1. Flow Physics

Since the first observation of the SBLI phenomenon about sixty years ago, significant progress has been achieved, both experimentally and computationally. Reviews of work carried out have been given previously by Hankey and Holden (1975), Adamson and Messiter (1980), and most recently by Delery (1999) and Dolling (2001). The work has covered a wide range of Mach numbers and Reynolds numbers, and various SBLI configurations. According to the free interaction concept first proposed by Chapman et al. (1958), the pressure rise at separation depends only on the incoming flow conditions, and not on the mechanism leading to separation. Likewise, for given freestream conditions, it has been found that the surface properties (pressure, shear stress, and heat-flux) are primarily dependent on the overall pressure rise experienced in the interaction, irrespective of how this pressure rise is generated. Thus, SBLIs arising from oblique shock impingement or from compression ramps have similar surface distributions of these properties.

Figure 2-1 illustrates a representative SBLI caused by the interaction of an incoming oblique shock-wave generated by a sharp wedge (shock generator) with a two-dimensional boundary-layer growing on a flat plate. This configuration contains the essential flow field features typical of all 2-D oblique SBLIs and has been studied extensively, both experimentally and numerically. In Figure 1, the subscript is applied to properties evaluated in the freestream, upstream of the plate, whereas (1) denotes the inviscid region behind the bow shock generated, in the hypersonic flow cases considered here, by viscous interaction at the leading edge of the plate (Korkegi, 1971). Region (2) is the inviscid region behind the impinging shock, while the subscript (3) denotes the inviscid region behind the shock reflection downstream of the interaction.

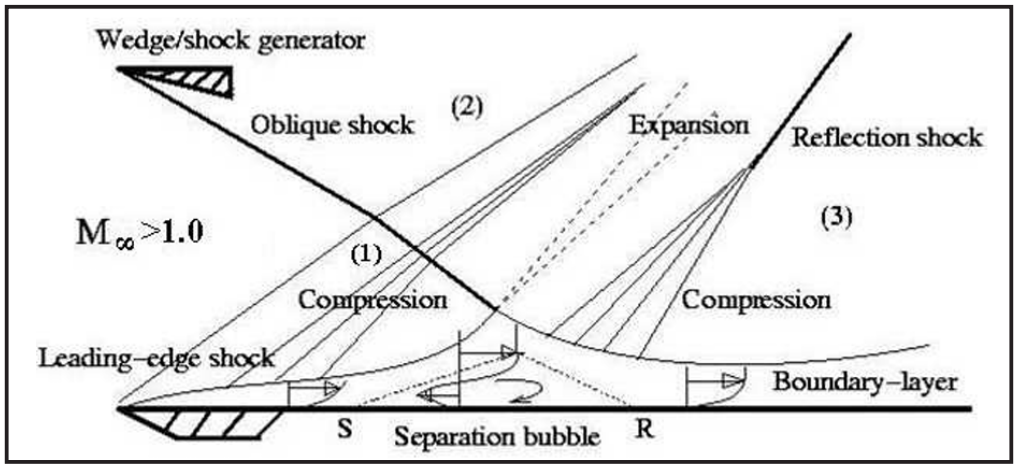

Figure 1: A sketch of laminar shock/boundary-layer interactions with the Freestream M > 1.0 inflow

Table 1: Parameter combinations of numerical investigation

case	symbols	Mach number, M_∞	Reynolds number, Re_{x0}	overall pressure ratio, $(p_3/p_1 p_3/p_1)$
1	Δ	7.87	1.81×10^6	4.81
2	O	7.73	0.51×10^6	1.32; 2.51; 4.40
3	*D*	6.85	0.78×10^6	8.35
4	*A*	6.85	0.25×10^6	2.27; 3.81; 5.86; 8.10
5	*o*	4.50	0.30×10^6	1.74; 2.91; 4.43
6	◦	2.00	0.30×10^6	1.25; 1.40; 1.63; 1.86

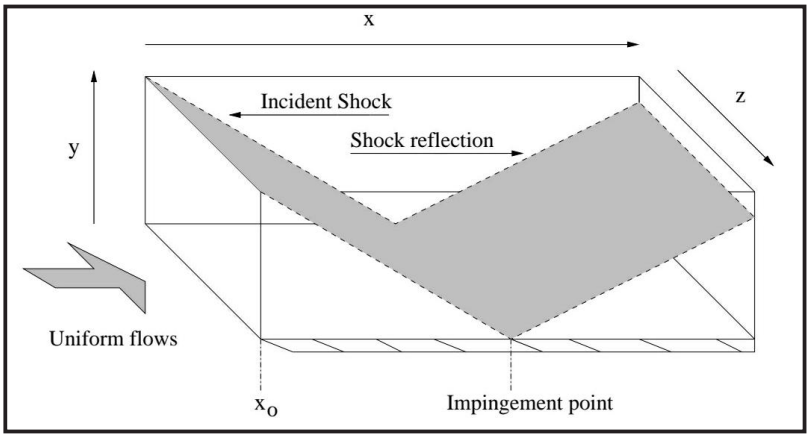

Figure 2: A sketch of the interaction domain

For a given freestream Mach number, M_∞, the strength of the impinging oblique shock-wave, represented by the shock angle β, ıtrolled by the wedge angle θ. The boundary-layer encountering the pressure increase p_3/p_1 (overall pressure ratio) across the interaction region is decelerated and thickened, and will separate if the shock is sufficiently strong (the zero-skin friction point is denoted as 'S'). As illustrated, the influence of the impinging shock extends upstream of the impingement point. Unlike the inviscid case, in which the impinging shock would be reflected from the wall, the interaction of the incident shock with the already separated boundary layer induces an expansion fan to maintain pressure continuity in the separated region. The expansion causes the downstream flow to turn towards the wall, where the flow reattaches (at the reattachment point denoted as 'R'). Consequently, a primary separation bubble is formed. Two compression zones, extending from the separation and reattachment regions, cause the pressure increase at the beginning and the end of the interactions. Over the separation region, there is a flattened pressure variation, hereafter referred to as the 'pressure plateau'. The general qualitative aspects of the interaction, as described above and illustrated in Fig. 1, apply to laminar, transitional, and turbulent SBLIs, but the size and severity (e.g., in terms of surface heat-flux enhancement) of the interaction depend on the state of the boundary-layer. In particular, as laminar boundary-layers are more prone to separation, for a given overall pressure ratio, the length of the separation bubble is much greater for laminar than turbulent boundary-layers, and the pressure plateau is more extensive. On the other hand, surface properties such as skin friction and heat transfer are much greater in transitional and turbulent interactions.

The 2-D numerical simulations carried out in this study cover a broad range of Mach numbers, from supersonic to hypersonic (see Table 1). Reynolds numbers were sufficiently low to expect that the boundary-layer growing over the flat plate in the absence of the SBLI would remain laminar. The Reynolds numbers quoted in Table 1 are based on the distance downstream of the leading edge of the flat plate at which the oblique shock would impinge on the wall in the absence of the boundary-layer. This distance is designated as x_0, as in Figure 2 of the interaction domain. The overall pressure ratio p_3/p_1, governed by the impinging shock strength, was treated as a variable parameter. Where possible, the results are compared with experimental and/or other numerical results and also analysed in terms of correlation

parameters proposed for supersonic SBLIs by Katzer (1989), derived from the earlier work by Chapman et al. (1958).

Pioneering experiments for this flow configuration were carried out by Chapman et al. (1958) and Hakkinen et al. (1959), who advanced the earlier experimental work of Liepmann (1946) and provided the basic physical understanding of SBLI phenomena in the two-dimensional laminar flow regime. The flow conditions for the work of Hakkinen et al. (1959) were M_∞ = 2.0 and Re ≈ 2.9×10^5. These experiments were also simulated numerically by Katzer (1989) and Wasistho (1998), and provide a supersonic flow benchmark for the simulations presented in this paper. Degrez et al. (1987) revisited the problem for M_∞ = 2.15 and Re ≈ 10^5, aiming for a complete experimental database by using more advanced measurement techniques. A complementary numerical solution was also performed in their study. Several experimental studies of 2-D laminar oblique SBLIs in the hypersonic regime have also been carried out, with Mach numbers ranging from 7.3 to 18.9 and Reynolds numbers from 1 x 10^5 to 25 x 10^5 (e.g., Needham and Stollery, 1966; Kaufman and Johnson, 1974; and Holden, 1978). Three-dimensional effects were investigated by Henckels et al. (1993) and Kreins et al. (1996) using high-resolution surface measurement techniques, in which the existence of longitudinal Görtler vortices was observed in the flow field downstream of the SBLIs. These experiments were carried out at Mach numbers of 6 and 8.7 with Reynolds numbers of approximately 9 x 10^5.

Numerical investigations of laminar hypersonic SBLI problems have also been carried out by Hodge (1977) and by Issa and Lockwood (1977). In general, the results agreed well with the wall pressure and heat-flux distributions for weak interactions, but not for strong interactions. Dömrose et al. (1996) carried out 2-D and 3-D numerical simulations, aiming to reproduce the experiments of Henckels et al. (1993). In these numerical simulations, Görtler vortices were observed downstream of the reattachment.

2.2. Method

A complete description of the numerical method used in the present study was given by Sandham et al. (2002) for a shock-free compressible turbulent channel flow. Using this code, the compressible unsteady 3-D Navier-Stokes (NS) equations are solved via a 4th-order central finite difference-TVD scheme for evaluating spatial derivatives and an explicit 3-step Runge-Kutta algorithm for time advancement. Other numerical techniques are also used, including entropy splitting of Euler terms, a Laplacian form for viscous terms, and a stable high-order boundary treatment. A Sutherland law viscosity variation is implemented with thermal conductivity evaluated via a fixed Prandtl number (0.72 for air and 0.70 for nitrogen). The fluid is assumed to behave as a thermally perfect gas with constant specific heat capacities in the ratio γ = 1.4. Readers are referred to Sandham et al. (2002) for detailed equations and numerical methods.

Yao et al. (2000) have demonstrated the capability of the same numerical method for flows containing shock-waves, and preliminary results of some of the present oblique SBLI simulations have also been presented elsewhere (Bura et al., 2001; Yao et al., 2002). The code has been developed specifically to investigate transitional/turbulent boundary-layer phenomena by direct numerical simulation (DNS). In the work presented here, however, the discussion is limited to steady, laminar SBLI simulations in 2-D. The solution is advanced in time until steady state conditions are achieved, as evidenced either by a rate of change of wall pressure less than 10^{-6} per time step, or until there are negligible changes in the flow properties of primary interest, such as separation lengths, wall shear stress, and heat-flux.

Time advancement was limited by stability requirements; the maximum CFL (Courant-Friedrichs-Lewy) conditions used were 1.0 for cases 1 – 4 (hypersonic inflow) and 2.0 for cases 5 – 6 (supersonic inflow). Convergence to a steady state required more iterations as the shock angle (corresponding to shock strength) was increased. This, in turn, increased the number of time units (non-dimensional time) required for the solution to converge to a steady state. A typical strong shock case (M_∞ = 6.85) took 300,000 iterations (≈ 8,000 time units) to converge. For all the computations reported here, the code used was configured to run on a single processor (SGI Origin 2000 computer).

2.2.1. Input Boundary Conditions

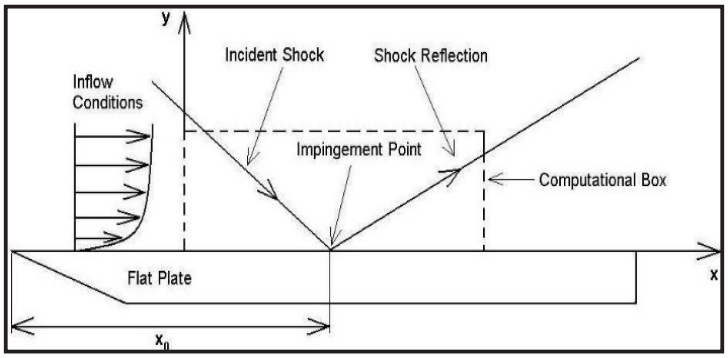

(a) Supersonic case

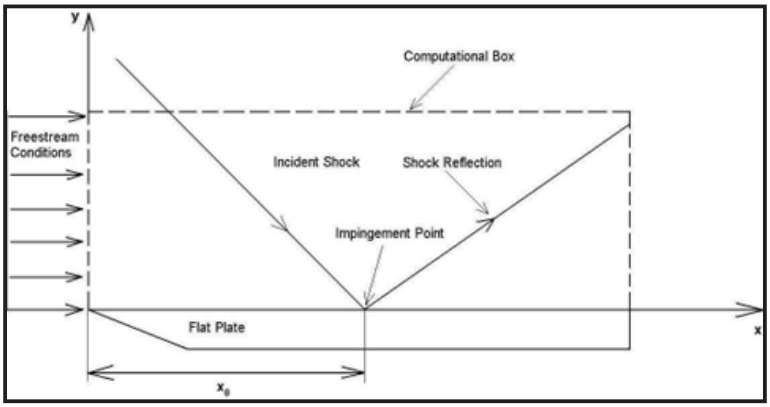

(b) Hypersonic case

Figure 3: Supersonic and Hypersonic Computational Domain (in dashed lines)

For each of the test cases considered in Table 2-1, the computational domain comprised a rectangular box, arranged in such a way that the oblique shock originated from near the top left-hand of the upper boundary and impinged near the middle of the lower (solid wall) boundary. Figure 3 shows the computational domain for both supersonic and hypersonic cases. The M_∞ = 2.0 simulation (case 6) is a repeat of that carried out originally by Katzer (1989) and Wasistho (1998), and is based on experiments performed by Hakkinen et al. (1959). This simulation was used as a benchmark. Hypersonic SBLI simulations were also carried out at Mach numbers of $M_\infty \approx 8.0$ (cases 1 and 2) and M_∞ = 6.85 (cases 3 and 4). The former were based on experiments performed by Kaufman and Johnson (1974), and the latter conditions were similar to those employed by Smith (1993) in his compression ramp experiments at the University of Southampton. The M_∞ = 4.5 simulations (case 5) were used as an intermediate between the supersonic and hypersonic simulations.

The boundary conditions applied differed between the supersonic and hypersonic simulations. For the supersonic cases (5 and 6), velocity and temperature boundary-layer profiles were prescribed at the inlet plane. These were generated by a separate self-similar compressible laminar boundary-layer analysis under the given freestream flow conditions (White, 1974). An adiabatic no-slip boundary condition was applied at the lower solid boundary. With these inflow conditions, viscous interaction at the leading edge of the plate was neglected, and region 1 is identical to the freestream conditions.

For the hypersonic cases (1 – 4), uniform inflow conditions were used, except for the point at the solid wall where a no-slip condition was applied. In this way, the boundary-layer growth from the leading edge of the flat plate was simulated, and the effects of viscous interaction near the leading edge of the flat plate were thus automatically taken into account, these being much more significant in the hypersonic cases. An isothermal cold wall (Tw = 300 K), with a no-slip condition, was applied at the lower solid boundary so that the wall heat-flux variation could be investigated.

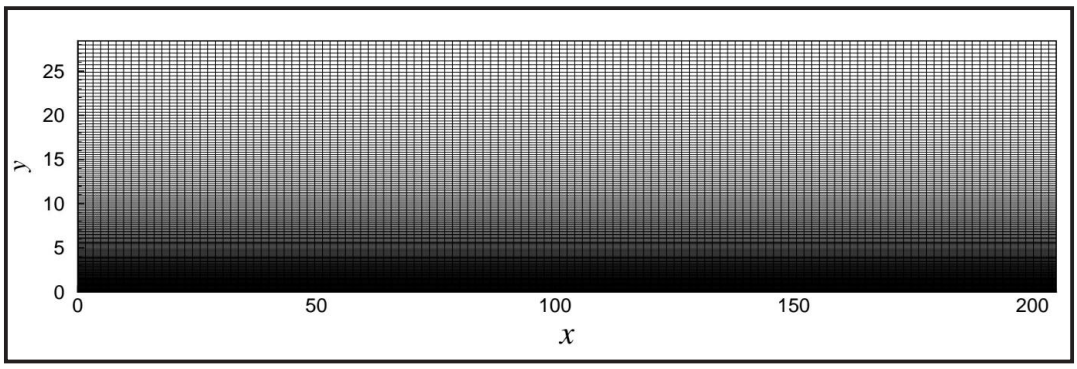

Figure 4: Grids employed for supersonic and hypersonic cases

Table 2: Grid Refinement Study

Case	M_∞	p_3/p_1	$L_x \times L_y$	$N_x \times N_y$	ΔL_{sep}	Δc_f	ΔS_t
2	7.73	4.40	456 × 48.58	128 × 192	28.83	BL	BL
				192 × 192	-2.2%	-2.2%	3.6%
				128 × 256	1.5%	0.8%	0.6%
4	6.85	5.86	205 × 24.91	128 × 192	BL	BL	BL
				192 × 192	-1.5%	0.4%	2.7%
				128 × 256	0.3%	0.4%	2.4%
5	4.50	2.91	340 × 30	128 × 128	BL	BL	-
				192 × 192	-0.4%	-0.4%	-
				128 × 192	1.1%	0.4%	-
6	2	1.40	400 × 115	151 × 128	BL	BL	-
				192 × 192	< 0.1%	< 0.1%	-
				192 × 192	2.3%	< 0.1%	-

For the hypersonic cases (1 – 4), uniform inflow conditions were used, except for the point at the solid wall where a no-slip condition was applied. In this way, the boundary-layer growth from the leading edge of the flat plate was simulated, and the effects of viscous interaction near the leading edge of the flat plate were thus automatically taken into account, these being much more significant in the hypersonic cases. An isothermal cold wall (Tw = 300 K), with no-slip condition, was applied at the lower solid boundary so that the wall heat-flux variation could be investigated.

In all cases, a characteristic boundary condition was used at the outlet plane to minimize any reflected waves. At the upper computational boundary, freestream quantities were given in front of the oblique impinging shock-wave. The latter was introduced at a given location by applying the exact shock jump properties corresponding to a particular wedge angle, which were calculated analytically. The test gas considered was air, except for the M_∞ = 6.85 cases (3 and 4), for which it was pure nitrogen.

2.2.2. Grid and Grid Refinement

The grids employed in this study had a uniform spacing in the streamwise (x-direction), but a non-uniform spacing in the wall-normal (y-direction), with clustering towards the wall in order to capture better the boundary-layer gradients. A conformal, orthogonal mapping was applied to the computational domain to affect the clustering, and the clustering parameter was varied to optimize the grid. This proved to be quite difficult for this configuration, as it is necessary not only to capture the gradients in properties within the boundary-layer but also to resolve correctly the oblique impinging and reflected shocks. The grids employed for both supersonic and hypersonic cases are shown in Figure 4.

Sensitivity of the numerical solution to the grids employed was investigated systematically for particular test cases. For the supersonic cases, the baseline grid had 151 points in the x-direction and 128 points in the y-direction. With this grid and the particular clustering parameter employed, there were approximately 20 – 30 points lying within the boundary-layer

at the inlet plane. Test simulations were also carried out separately with 50% extra cells in the x- and y-directions. The grid refinement results obtained, shown in Table 2, were almost identical to those obtained with the baseline grid, indicating that a near grid-independent solution had been obtained.

Grid refinement and optimization for the hypersonic cases were more challenging. It was thought that this was due to the difficulty in simulating accurately the initial boundary-layer growth near the leading edge of the plate, particularly as this is subject to the effects of viscous interaction. This will be discussed further in Section 3.2. Ultimately, an optimized grid was derived, comprising 128 × 192 points in the x- and y-directions, respectively. With this grid, typically about 40 – 60 points lay within the boundary-layer just upstream of the interaction. This grid was used as a baseline, but again, test simulations were carried out with 50% extra points in, separately, the x- and y-directions. Except near the leading edge of the plate, these produced negligible changes compared with the baseline case, which was therefore considered to produce a near grid-independent solution. The grid refinement study for the hypersonic case is also shown in Table 2.

3. Result and Analysis

Oblique SBLI simulations were carried out for the range of conditions described in Table 1. In the following sections, particular attention is drawn to the simulations at M_∞ = 2.0 and M_∞ = 7.73, and the results obtained are compared with available experimental data at these two conditions. An attempt is then made to correlate data concerning certain features of the flow field, using parameters that have been proposed previously by Katzer (1989), who derived them from the earlier work by Chapman et al. (1958). Here, we extend the use of these parameters to higher Mach numbers to determine whether the flow field under these conditions behaves according to the free interaction concept. An analysis of peak surface heat-flux data is also carried out using correlation parameters derived previously by Hung (1973).

3.1. Simulations at M_∞ = 2.0

Figure 5 shows Mach number contours for case 6 with p_3/p_1 = 1.40. The incoming oblique shock follows the predefined shock angle (β = 32.58°) and impinges on the middle of the lower computational boundary, as required. In this case, the impinging shock is sufficiently strong to cause the boundary-layer to separate. The simulations reproduce the main features, as illustrated in Figure 5, and are in agreement with the experimental observations. Some reflected waves appear around the upper/outflow corner of the computational boundary, which is due to the fixed flow properties used for the upper boundary after the shock. Similar reflected waves also occurred in the simulation of Wasistho (1998) for the same configuration. These features do not influence the flow near the solid boundary.

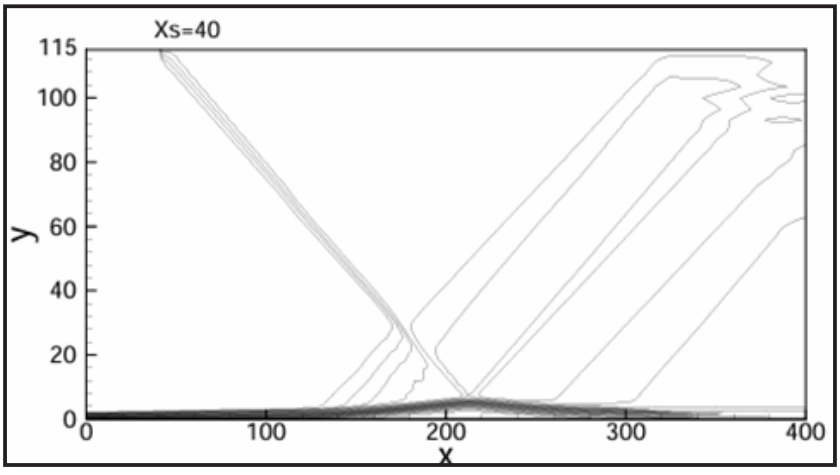

Figure 5: Mach number contours for M_∞ = 2.0 (case 6) with p_3/p_1 = 1.40

Figures 6 and 6 show a comparison of the wall pressure (p_w) and skin friction coefficient (c_f) for the above case with previous simulations (Katzer, 1989 and Wasistho, 1998) and experiment (Hakkinen et al., 1959). The wall pressures have been normalized by the freestream

pressure at the inflow plane, whereas c_f is defined conventionally from the wall shear stress. It is clear that as the boundary-layer thickens and separates due to the shock impingement, the wall pressure rises and reaches a plateau before increasing again at reattachment.

Simultaneously, the skin friction reduces and becomes negative (indicating separation and recirculation). A secondary minimum in c_f is also observed just ahead of the rise associated with reattachment. These variations are typical of separation due to a relatively strong shock/boundary-layer interaction. They are in agreement with previous numerical results and match fairly well the experimental results obtained for this configuration, particularly for the pressure variation. However, compared with the experimental data, the skin friction is underpredicted (particularly near reattachment) by all of the numerical simulations.

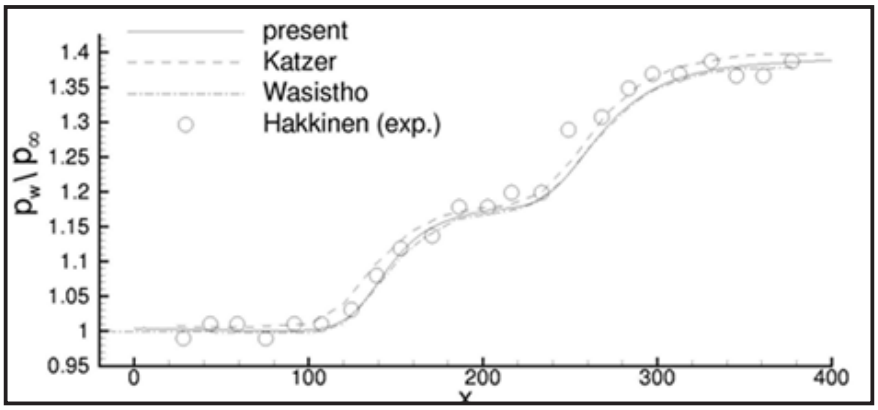

Figure 6: Comparison of simulations and experiment for M_∞ = 2.0 and p_3/p_1 = 1.40: wall pressure distributions

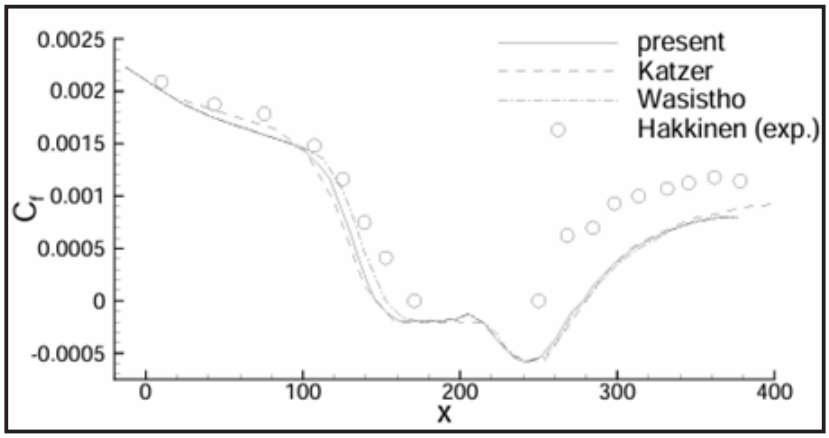

Figure 7: Comparison of simulations and experiment for M_∞ = 2.0 and p_3/p_1 = 1.40: skin friction distributions

The effect of varying the impinging shock strength (and hence the overall pressure ratio) was explored. A subdomain is used for plotting streamlines. Figure 8 shows the streamline traces for a weak impinging shock (p_3/p_1 = 1.25). In this case, a small symmetric separation bubble is formed around the impingement point. The separation bubble increases in size as the shock strength is increased, in Figures 3-5 and 3-6, and becomes asymmetric in shape. For the strongest interaction illustrated (p_3/p_1 = 1.65), a small secondary vortex embedded inside the primary vortex is also evident. This feature arises from the inability of the reversed flow to negotiate the slight adverse pressure gradient within the primary separation bubble and also grows in size as the impinging shock strength is further increased. Note that the streamline traces for the p_3/p_1 = 1.86 case are not shown here but follow the same trend. These results agree with those of Shen et al. (2000), who used a different numerical approach for the same configuration.

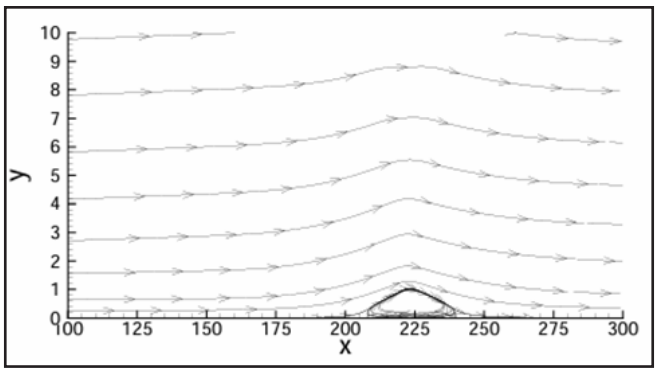

Figure 8: Streamline traces for M_∞ = 2.0 inflow, p_3/p_1 = 1.25

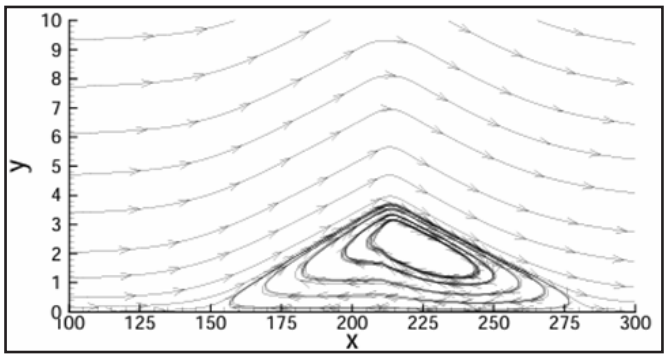

Figure 9: Streamline traces for $M_\infty M_\infty$ = 2.0 inflow, $p_3/p_1 p_3/p_1$ = 1.40

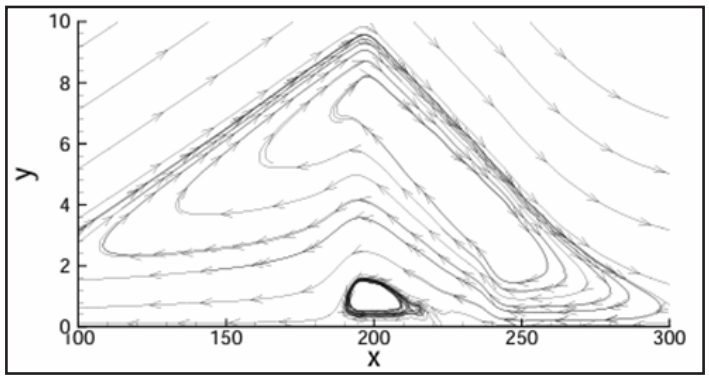

Figure 10: Streamline traces for $M_\infty M_\infty$ = 2.0 inflow, $p_3/p_1 p_3/p_1$ = 1.65

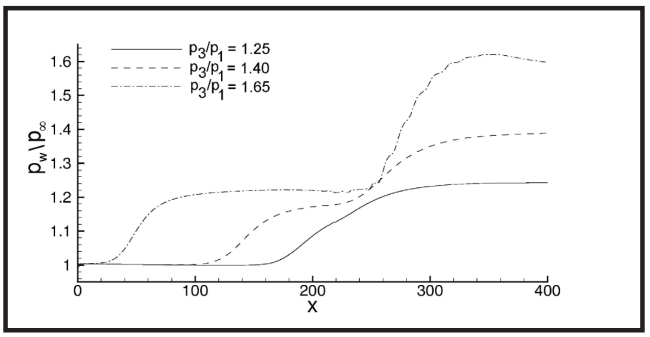

Figure 11: Comparison of case 6 at different overall pressure ratios; wall pressure distributions

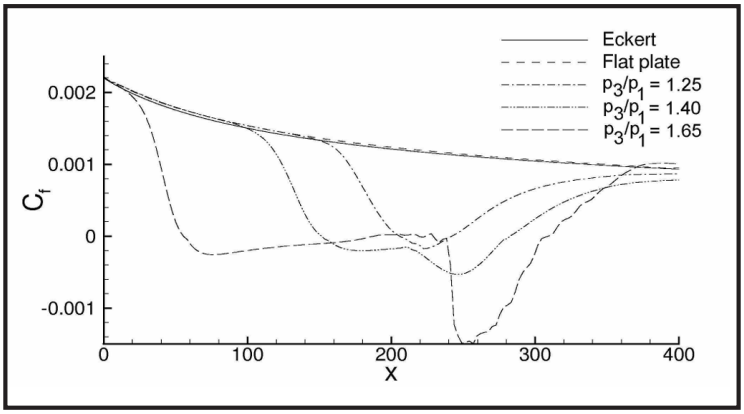

Figure 12: Comparison of case 6 at different overall pressure ratios; skin friction distributions

Figures 11 and 12 compare the wall pressure and skin friction coefficient distributions for the cases illustrated in Figures 3-4, 3-5, and 3-6. The pressure distributions illustrated in Figure 11 indicate that there is no clear pressure plateau for the weak interaction case, but the plateau develops as the impinging shock strength is increased. The plateau pressure increases only slightly as the shock strength is increased, whereas the pressure at reattachment rises sharply.

Figure 12 shows the corresponding skin friction coefficient (c_f) distributions. Flat plate results obtained from theory via the reference temperature method of Eckert (1955) and by numerical simulation are also plotted for comparison. The latter agrees well, again confirming that the inflow conditions and the undisturbed boundary-layer growth are simulated correctly. It is clear that with shock impingement, the flow separation increases from incipient to extensive in size. The skin friction distribution for the strongest shock case illustrated confirms the presence of a secondary vortex. In these supersonic simulations, the shear stress near reattachment rises to levels similar to those in the undisturbed flow.

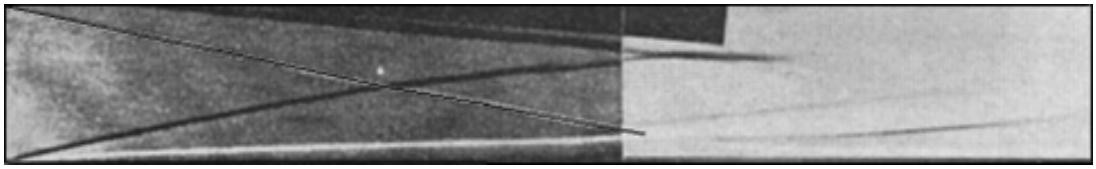

(a) Schlieren photograph

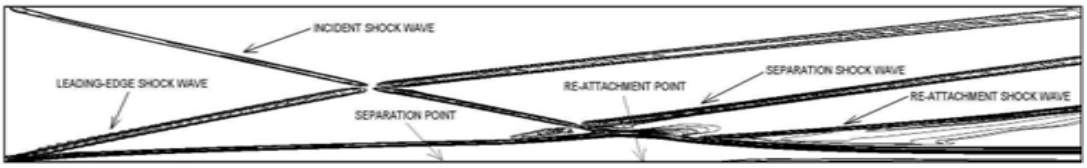

(b) Density gradient contours

Figure 13: Schlieren photograph (a) and density gradient contours (b) for M_∞ = 7.73 (case 2) at a wedge angle of 5°

3.2 Simulations at M_∞ = 7.73

Simulations were also carried out at the freestream M_∞ = 7.73 (see Table 1), and the results were compared with experimental data obtained by Kaufman and Johnson (1974) at these conditions to ascertain the validity of the present numerical method for oblique shock SBLIs in the hypersonic regime.

Figure 13 (a) shows the schlieren image obtained by Kaufman and Johnson for M_∞ = 7.73 with a wedge angle of 5° (shock angle = 11.08°, p_3/p_1 = 4.40). The Reynolds number Re_{x0} was 0.51 x 10^6. The wedge shock generator is visible at the top of the image; the impinging shock emerging from the top left-hand corner is also visible (note: the image has been enhanced to make this feature visible as a feint black line). On the lower boundary, the bow shock growing from the leading edge of the plate is clearly evident, along with the edge of the

boundary-layer growing behind it. Although the flat plate is at zero incidence with respect to the freestream flow, the bow shock is generated as a result of viscous interaction with the developing boundary-layer.

Further downstream, after the impinging shock passes through the bow shock (with only slight refraction), it interacts with the boundary-layer, causing it to separate. Although the features in this region are not well-defined, a separation shock and reattachment shock can be observed, along with the reattaching boundary-layer.

Figure 13 (b) is the equivalent image obtained from the numerical simulation, plotted as contours of density gradient. All the flow features described above are visible and appear to match the experimental image and are similar to those sketched in Figure 5. However, it is well-known that the density field visualized by schlieren techniques is not a particularly good basis for validating numerical results since, in most cases, the comparison is qualitative rather than quantitative.

Figures 14, 15, and 16 illustrate the surface pressure, skin friction, and heating distributions and compare the numerical and experimental results for this case. In each, the x-axis corresponds to the distance from the leading edge of the flat plate, in millimeters. However, there is no experimental result available for the skin friction distribution, so a comparison with the simulation result is not possible. In Figure 14, the pressure has been normalized by the freestream value at the inlet plane, whereas in Figure 16, the dimensional value of the heat transfer coefficient (defined conventionally from the wall heat-flux and the adiabatic wall temperature) is plotted.

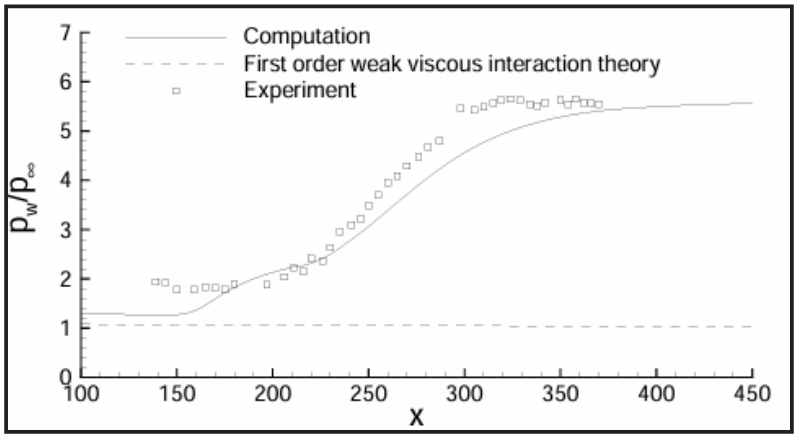

Figure 14: Wall pressure distributions for $M_\infty M_\infty$ = 7.73 (case 2) at a wedge angle of 5°

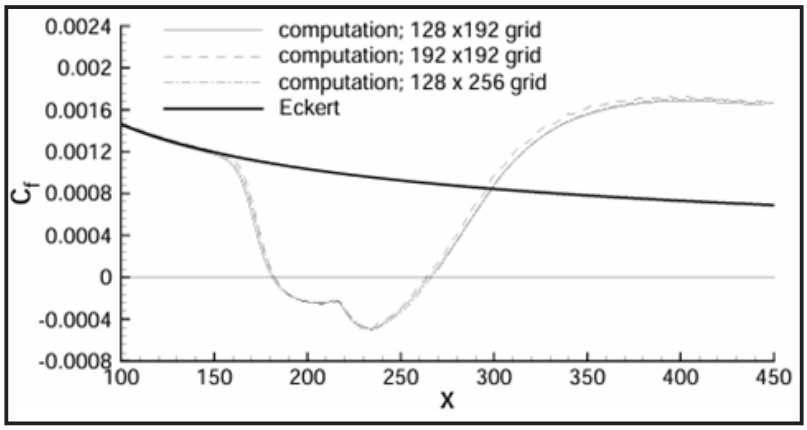

Figure 15: Skin friction distributions for M_∞ = 7.73 (case 2) at a wedge angle of 5°

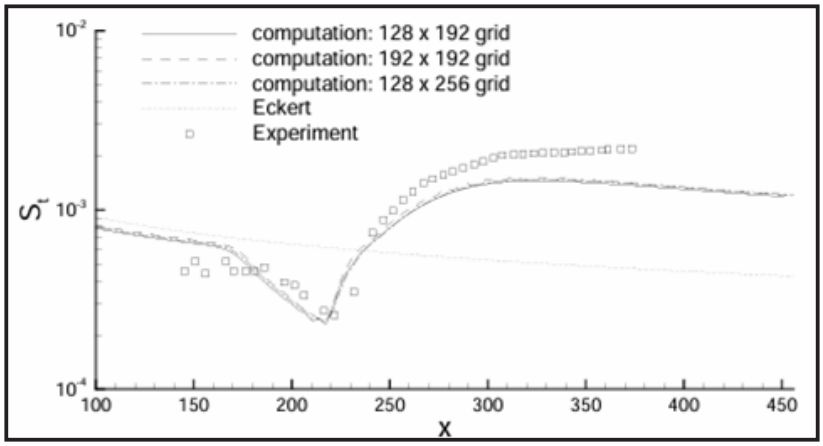

Figure 16: Wall heating distributions for M_∞ = 7.73 (case 2) at a wedge angle of 5°, (128 x 192 points)

Considering first the pressure distribution, the agreement between the experimental and numerical results is evidently poorer than that in the Mach 2 simulations. Viscous interaction effects near the leading edge appear to be much stronger than predicted by first-order interaction theory (Anderson, 1989). In this region, the measured pressures are significantly greater than those predicted from the numerical simulations. This is surprising given the good agreement between the experimental and numerically generated schlieren images, but it may indicate inadequate grid resolution in this region, since fully resolving the sharp leading edge is not possible.

Overall, the simulations appear to underpredict the measured wall pressures. The distribution obtained via the numerical simulation is similar to that described earlier for the supersonic case, with a tendency towards a plateau in the separation zone. In the experimental case, the initial rise in pressure marking the onset of the interaction occurs much further downstream (x = 200 mm), and there is no clear indication of a pressure plateau.

From the skin friction plot in Figure 15, it can be seen that, according to the numerical results, separation originates at x = 175 mm and ends at about x = 270 mm. The simulation predicts a well-separated flow, including the presence of a second minimum in c_f that was also found in some of the M_∞ = 2.0 simulations with strong impinging shocks. Note, however, that the peak skin friction after reattachment is significantly higher than in the undisturbed flow, unlike the results obtained at M_∞ = 2.0.

The corresponding heating distributions plotted in Figure 16 also indicate discrepancies between the experimental and numerical data (note that the heat transfer coefficient has been plotted using a logarithmic scale). In contrast to the wall pressures, the numerical heating values exceed the experimental data in the undisturbed region upstream of the interaction. Both are less than the theoretical heating distribution obtained for the undisturbed flat plate via the reference temperature method of Eckert (1955). In the numerical case, it was thought that the grid may have been insufficiently fine to resolve adequately the temperature gradients in the boundary-layer near the leading edge. However, as can be seen in Figure 16, the heat-flux distributions obtained for grids with 50% more points in both streamwise and normal directions are almost negligibly different from those of the baseline case.

This observation is also evident in the skin friction distribution, Figure 15. There is no obvious explanation for the comparatively low heat-fluxes measured experimentally in this region, other than possibly indicating a systematic error in either the heat-flux measurements or the measurement of the tunnel operating conditions. Note that the grid refinement study was only carried out for the heat-flux and skin friction distributions, but not for the pressure distribution, due to the greater sensitivity of wall surface parameters to grid refinement compared to the pressure distribution.

The onset of the interaction (indicated by the sudden reduction in heat-flux as the boundary thickens and separates) occurs further upstream numerically than was observed

experimentally, as noted in the pressure distributions. Similarly, the heating levels measured experimentally near the reattachment region exceed those predicted numerically. This difference is even more remarkable, given that the measured heat-fluxes in the upstream undisturbed region were less than those predicted numerically. This observation will be discussed further in Section 3.3.

Similar results were obtained with simulations carried out with different wedge angles (with correspondingly different pressure ratios), although it was noted that the onset of the interaction appeared to be in better agreement with the experimental observations at low wedge angles. A test case was also carried out at a higher Reynolds number of 1.81 x 10^6, at M_∞ = 7.87 and with p_3/p_1 = 4.81 (Case 1). Again, similar results were obtained with corresponding discrepancies between the measured and predicted pressure and heating distributions, although the difference between the measured and predicted heat-fluxes in the reattachment region appeared to be slightly greater in the higher Reynolds number case.

3.3 Correlation of Results

Numerous correlations derived from the free interaction concept have been proposed. For the present cases, the correlations used by Katzer (1989) were applied. He numerically studied two-dimensional supersonic SBLIs in a similar configuration to the present case under the influence of different Mach numbers ($1.4 \le M_\infty \le 3.4$), Reynolds numbers ($0.1 \times 10^6 \le Re \le 0.6 \times 10^6$), and (weak) shock strengths on an adiabatic flat plate. In particular, he confirmed that the wall shear stress at the beginning of the interaction region and the Mach number at the edge of the boundary-layer govern the separation and plateau pressures. This present work also applies the correlations used by Katzer to hypersonic SBLIs with isothermal (cold) walls (see Table 2-1).

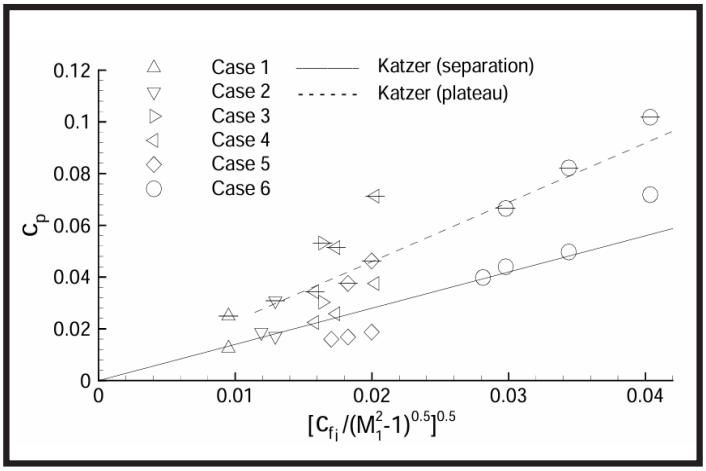

Figure 17: Pressures at separation points and plateau regions. Plateau pressure symbols have short horizontal lines

Note that there are 16 cases in Table 1. However, of these, only 14 cases produced a fully separated flow, and only 11 cases exhibited a well-developed pressure plateau. Hence, not all cases are represented in the following correlation plots.

Figure 17 shows the pressure coefficients, c_p, at the separation point and in the plateau region of the present cases, plotted according to the correlation proposed by Katzer, Eq. (1), below.

$$c_p = \frac{2}{\gamma M_1^2}\left(\frac{p}{p_2} - 1\right) = P\left(\frac{c_{f_1}}{\sqrt{(M_1^2 - 1)}}\right)^{\frac{1}{2}} \quad (1)$$

In the above expression, the constant of proportionality P is applied to the separation point (i.e., $P = P_s$ when $p = p_s$, the local pressure at the separation point), and also to the plateau region (i.e., $P = P_p$ when $p = p_p$, the plateau pressure). Following the procedure adopted by Katzer, the wall skin friction coefficient is obtained from a modified Blasius expression (

$c_{f_1} = 0.664/\sqrt{Re_{x1}/C}$), where $x1$ is the position at the beginning of the interaction region and C C is the Chapman-Rubesin constant (defined as $C = \sqrt{(\mu_\omega T_\infty)/(\mu_\infty T_\omega)}$). Note that the pressure coefficients are defined with respect to the inviscid conditions just upstream of the interaction (i.e., region 1 in Figure 1) rather than the free stream conditions.

In his numerical simulations of supersonic SBLIs with relatively weak impinging shocks, Katzer found that $P_s = 1.40$ and $P_p = 2.30$, and that these values compared favorably with experimental and theoretical values derived by other researchers. Katzer's correlation with these values of P_s and P_p is also plotted in Figure 27. Note that Katzer's correlation for the plateau regions starts from approximately 0.013 on the abscissa. It is apparent that our present numerical data, obtained over a wider range of Mach numbers and with both adiabatic and non-adiabatic walls, agree well with this correlation, albeit with somewhat greater scatter than exhibited by Katzer's data. This indicates that the free interaction concept applies to the cases being considered here.

The data plotted in Figure 27 show that, as the Mach number is increased, the P_s at separation and in the plateau region decreases. However, considering the definition of the pressure coefficients with respect to Mach number, it becomes evident that the actual pressure ratios at separation and in the plateau region (p_s/p_1 and p_p/p_1, respectively) increase with Mach number. Because these pressure ratios are always greater than unity, and c_{f_1} is always positive, the origin in Figure 27 is approached only when M_1 (and hence M_∞) becomes very large.

The aforementioned correlations were made possible using theoretical considerations based on the free interaction concept, which identifies the dependent parameters (e.g., M_1, c_{f_1} , etc.), while the constants can be derived empirically from experiments or numerical simulations. The concept has also been used as a guide for establishing other empirical correlations. Needham and Stollery (1966), for example, were able to correlate plateau pressures from a large number of previous experiments for separated laminar flows using the equation below.

$$c_{p_p} = 3c_{f_1}^{\frac{1}{2}}(M_1^2 - 1)^{-\frac{3}{4}} \quad (2)$$

The correlation shown in Eq. (2) covers a wider range of Mach number, $2 \le M_1 \le 16$, and includes geometries such as incident shocks, wedges, and forward-facing steps. Compared to Eq. (3-1) used for correlating data in Figure 27, Needham and Stollery's correlation (Eq. (3-2)) indicates a similar dependence on $\boldsymbol{c_{f_1}}$, but gives stronger emphasis to the effect of Mach number. However, when all the plateau pressure data shown in Figure 27 were plotted using the latter correlation, the plot produced more scatter than that shown in Figure 3-13. Hence, it is concluded that for the present cases, Eq. (3-1) provides a better correlation of the plateau pressure data.

Figure 18 shows the influence of Mach number and shock strength on the length of the separation bubble l_B, normalized by δ_0^* (the displacement thickness of an undisturbed boundary-layer at the position of the shock impingement point, x_0). It can be seen that the bubble length increases with increasing shock strength, p_3/p_1, as described earlier. The intersections of the plotted lines with the abscissa show that separation occurs only when the shock strength is larger than a certain threshold value, p_{inc}, which appears to increase with increasing Mach number. It also appears that the separation length decreases (for a given overall pressure ratio) with an increase in Mach number.

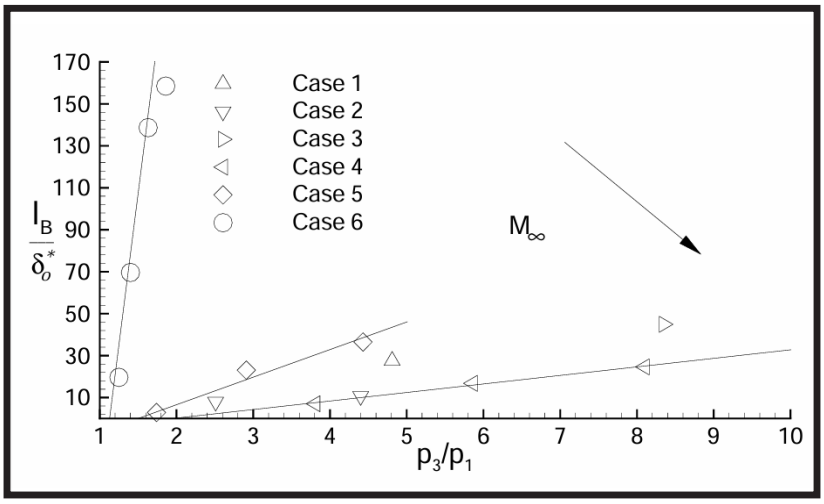

Figure 18: Separation bubble length, influence of the Mach number and shock strength

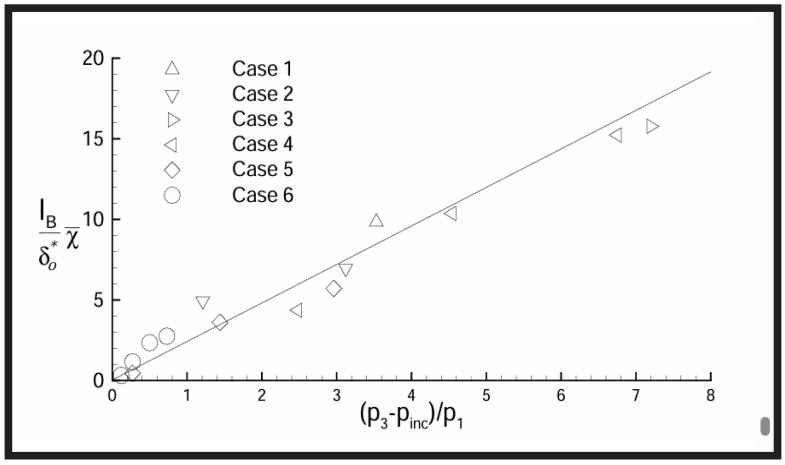

Figure 19: Separation bubble length, correlation of Katzer (1989)

There is also a suggestion that increasing the Reynolds number, with the Mach number fixed, increases the normalized separation length, although with only two significant data points (at M_∞ = 6.85 and 7.87), it is difficult to be conclusive. Nevertheless, such a trend would be consistent with the free interaction theory, exemplified by Eq. (3-1), since an increase in Reynolds number would result in a reduction of the skin friction coefficient, c_{f_1}, with a consequent reduction in the pressure coefficient at separation, c_{p_s}, at a given Mach number.

For his supersonic SBLI cases (with relatively low overall pressure ratio, p_3/p_1, or shock strength), Katzer showed that the normalized separation length, when multiplied by the viscous interaction parameter ($X = M_\infty^3\sqrt{C/Re_x}$), could be linearly correlated in terms of the overall pressure rise ($(p_3 - p_{inc})/p_1$). The data obtained from the present simulation over a wide Mach number range and with relatively high overall pressure ratios, as plotted in Figure 3-15, also appear to be well correlated by these parameters. However, the gradient of the straight line of best fit for the present data is about 24, whereas that for Katzer's data was 44. A close inspection of the present case 6 (M_∞ = 2.0) data reveals that the local gradient at low overall pressure ratios is higher and closer to Katzer's, but this does not extend to higher Mach number cases. This suggests that instead of a straight line fit, correlating the data using a power-law function would be more appropriate, as suggested by Kaufman and Johnson (1974).

The power-law function of best fit to the present data is given by:

$$\frac{l_B}{\delta_0^*}\bar{X} = 2.74\left[\frac{p_3 - p_{inc}}{p_i}\right]^{0.90} \quad (3)$$

It is notable that the exponent is only slightly less than unity.

The prediction of peak heating rates in the reattachment region represents a practical engineering problem. Hung (1973) proposed several correlations for peak heating rates in laminar, transitional, and turbulent interactions induced by incident shocks or compression corners. The correlations comprise power-law relations between the ratio of the peak values of pressure and heating to their undisturbed values, of the general form:

$$\left(\frac{\dot{q}_i}{\dot{q}_u}\right) = c\left(\frac{p_i}{p_u}\right)^n \quad (4)$$

where subscripts i and u denote interaction and undisturbed values, respectively, at the location of the peak heat-flux. Here, c and n are constants, whose values differ according to the boundary-layer state in the vicinity of the interaction.

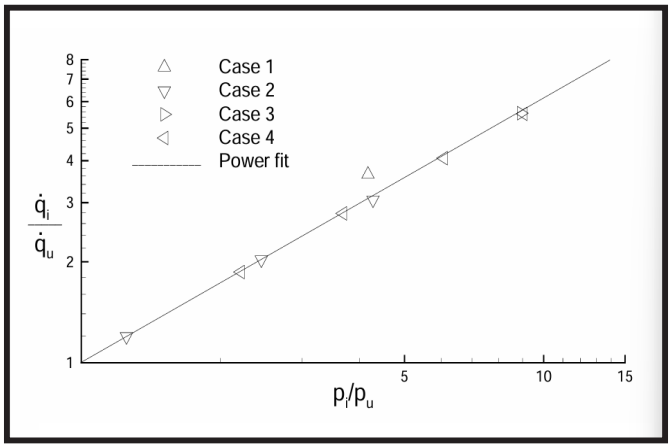

Figure 20: Peak heating correlation in terms of overall pressure ratio

Figure 20 is a plot of the peak heat-flux ratio, $\dot{q}_i/\dot{q}_u$, against the peak pressure ratio, p_i/p_u , for the present hypersonic simulations. Note that simulation cases 5 and 6 (with supersonic inflow conditions) are excluded from this figure because they concern interactions with an adiabatic wall. It can be seen that the heating data correlate well, with the line of best fit giving:

$$\left(\frac{\dot{q}_i}{\dot{q}_u}\right) = \left(\frac{p_i}{p_u}\right)^{0.78} \quad (5)$$

The exponent $n = 0.78$ is close to the value of $n = 0.7$ quoted by Hung (1973) for purely laminar interactions. Hung (1973) reviewed a range of heating correlations proposed by other researchers and observed a wide spread of results, which he attributed to previously unrecognized transitional effects. Most of these correlations (including those proposed by Hung himself) assume that $c = 1$, as we have found in our present results. However, some of the correlations reviewed by Hung were based not on the peak/undisturbed pressure ratio, but on the peak/freestream pressure ratio (p_i/p_∞). We have noted that if our peak heating data are correlated using the latter pressure ratio, c is less than unity ($c = 0.86$), but the exponent remains unchanged at $n = 0.78$. In either case, heating correlations of this kind are often convenient to use because they offer a simple method for estimating approximate peak heating values in such interference zones from the pressure distribution alone.

4. Conclusions

Oblique SBLI simulations have been carried out in the present work, covering a wide range of Mach numbers and overall pressure ratios. Features such as the separation and plateau pressures and the length of the separation bubble were correlated in terms of parameters developed previously by other researchers for supersonic SBLIs, but have been extended here into the hypersonic regime. The results obtained at M_∞ = 2.0 agree well with previous simulations by other researchers and reasonably well with available experimental data. In contrast, the agreement with experimental data at M_∞ = 7.73 is relatively poor. In particular, the interaction appears to commence further upstream than observed experimentally, and the wall heat-fluxes in the reattachment region are underpredicted by the numerical simulations.

Similar observations have been made by other researchers who have carried out hypersonic 2-D SBLI simulations. For example, Amaratunga et al. (1998) and Navarro-Martinez (2002) have attempted to simulate the flat plate-compression ramp experiments carried out by Smith (1993), in which unexpectedly high heat-fluxes were observed in the reattachment region on the compression ramp. From this work, it has become clear that 2-D laminar simulations generally overpredict the separation length and underpredict the heat-flux at reattachment. Navarro-Martinez has carried out further 3-D simulations that allow for the effects of lateral venting from the separation bubble. This has partially resolved the issue concerning overprediction of the separation length, but has had relatively little effect on the reattachment heat-flux. Localized 3-D effects (Görtler vortices) have also been shown to produce local streamwise increases in heat-flux in the reattachment region, but again, this has failed to fully resolve the discrepancy between the measured and predicted heat-fluxes.

In the present case, the experiments of Kaufman and Johnson (1974) were likely influenced by lateral venting, since the aspect ratio of the flat plate they employed was rather small (0.38). This may well help explain the observed differences between the measured and predicted onset of the interaction. However, it is probable that, just as in the compression ramp case described above, the observed discrepancy in the heating distribution is too large to be accounted for solely by the influence of 3-D effects.

Kaufman and Johnson admit the possibility of the separated shear layer undergoing transition in some of their experiments; if so, this would have the effect of reducing the separation bubble length and increasing the heat-flux at reattachment. In order to test this hypothesis, further 3-D unsteady simulations have recently been performed to investigate the propensity of the boundary-layer or separated shear layer to undergo transition in response to small, artificially applied perturbations.

As a final comment, it is now widely recognized that validation of 2-D numerical simulations by comparison with experiments should, if possible, be carried out with an axisymmetric configuration, free of the influence of the finite-span effects noted above.

Acknowledgements

This work was carried out with support from the UK Engineering and Physical Sciences Research Council (EPSRC) and the UK Defense Science and Technology Laboratory (DSTL).

References

References

Adamson, T.C. Jr., and Messiter, A.F.: Analysis of two-dimensional interactions between shock waves and boundary layers. Ann. Rev. Fluid Mech. 12, (1980) 103-138.

Amaratunga, S., Tutty, O.R., and Roberts, G.T.: Numerical predictions of hypersonic flow over a 2-D compression ramp. J.Spacecraft and Rockets 35(2), (1998) 230-232.

Anderson, J.D., Hypersonic and high temperature gas dynamics (McGraw-Hill, 1989).

Bura, R.O., Roberts, G.T., Sandham, N.D., and Yao, Y.F.: Simulation of hypersonic shock-wave/boundary-layer interactions. In: Proc. of the 23rd Int. Symp. on Shock Waves (ISSW23) (Lu, Frank K. (ed.), Forth Worth, Texas, USA (2001) 1371-1377.

Chapman, D.R., Kuehn. D.M. and Larson, H.K.: Investigation of separated flows in supersonic and subsonic streams with emphasis on the effect of transition. NACA Report 1356

(1958).

Degrez, G., Boccadoro, C.H. and Wendt, J.F.: The interaction of an oblique shock wave with a laminar boundary layer revisited. An experimental and numerical study. Journal of Fluid Mechanics. 177, (1987) 247-263.

Delery, J.M. and Panaras, A.G.: Shock wave boundary-layer interactions in high Mach number flows. AGARD Advisory Report No.319 (AGARD AR-319) 1, (1996) 2-1 to 2-61.

Delery, J.M.: Shock phenomena in high speed aerodynamics: still a source of major concern. The Aeronautical Journal 1, (1999) 19-34.

Dolling, D.S.: Fifty years of shock-wave/boundary-layer interaction research: what next? AIAA Journal 39(8), (2001) 1517-1531.

Domröse, U., Krause, E., and Meinke, M.: Numerical simulation of laminar hypersonic shock-boundary layer interaction. Z. Flugwiss. Weitraumforsch 20(2), (1996) 89-94.

Eckert, E.R.G.: Engineering relations for skin friction and heat transfer to surfaces in high velocity flows. Journal of the Aeronautical Sciences 22, (1955) 585-587.

Hakkinen, R.J., Greber, I., Trilling, L., and Abarbanel, S.S.: The interaction of an oblique shock wave with a laminar boundary layer. NASA Memo 2-18-59 W (1959).

Hankey, W.L. and Holden, M.S.: Two-dimensional shock wave-boundary layer interactions in high speed flows. AGAR- Dograph No.203 (1975).

Henckels, A., Kreins, A.F., and Maurer, F.: Experimental investigations of hypersonic shock-boundary layer interaction.

Z. Flugwiss. Weitraumforsch 17(2), (1993) 116-124. Hodge, B.K.: Prediction of hypersonic laminar boundary-layer/shock-wave interactions. AIAA Journal 15(7), (1977) 903-904.

Holden, M.S.: A study of flow separation in regions of shock wave-boundary layer interaction in hypersonic flow. AIAA Paper 78-1169 (1978).

Holden, M.S.: A review of aerothermal problems associated with hypersonic flights. AI-AA Paper 86-0267 (1986).

Hung, F.T.: Interference heating due to shock wave impingement on laminar boundary layers. AIAA paper 73-678 (1973).

Issa, R.I. and Lockwood, F.C.: On the prediction of two-dimensional supersonic viscous interactions near walls. AIAA Journal 15(2), (1977) 182-188.

Katzer, E.: On the lengthscales of laminar shock/boundary-layer interaction. Journal of Fluid Mechanics. 206, (1989) 477-496.

Kaufman, L.G.II and Johnson, C.B.: Weak incident shock interactions with Mach 8 laminar boundary-layers. NASA TN D-7835 (1974).

Korkegi, R.H.: Survey of viscous interactions associated with high Mach number flight. AIAA Journal 9(5), (1971) 771-784.

Kreins, A.F., Henckels, A., and Maurer, F.: Experimental studies of hypersonic shock induced boundary layer separation.

Z. Flugwiss. Weitraumforsch 20(2), (1996) 80-88.

Liepmann, H.W.: The interaction between boundary layer and shock waves in transonic flows. Journal of Aerospace Sciences 13(12), (1946) 623-638.

Navarro-Martinez, S.: Numerical simulation of laminar flow over hypersonic compression ramps. PhD thesis, University of Southampton (2002).

Needham, D.A. and Stollery, J.L.: Boundary-layer separation in hypersonic flow. AIAA Paper 66-455 (1966).

Sandham, N.D., Li, Q., and Yee, H.C.: Entropy splitting for high-order numerical simulation of compressible turbulence. Journal of Computational Physics 178(2), (2002) 307-322.

Shen, Y., Wang, R., and Liao, H.: A new numerical study of the shock/boundary-layer interaction. Int. J. Numer. Methods in Fluids 33, (2000) 23-34.

Smith, A.J.D.: The dynamic response of a wedge separated hypersonic flow and its effects on heat transfer. PhD thesis, University of Southampton (1993).

Wasistho, B.: Spatial direct numerical simulation of compressible boundary layer flow. Ph.D thesis, University of Twente, Netherlands (1998).

White, F.M., Viscous fluid flow (McGraw-Hill, 1974).

Yao, Y.F., Lawal, A.A., Sandham, N.D., Wolton, I.C., Ashworth, M., and Emerson, D.R.: Massively parallel simulation of shock/boundary-layer interactions. In: Proc. Inter Conf. of Applied Computational Fluid Dynamics, Beijing, China (2000) 728-735.

Yao, Y.F., Bura, R.O., Sandham, N.D., and Roberts, G.T.: Time-accurate simulation of supersonic and hypersonic laminar shock/boundary-layer interactions. In: Proc. CEAS Aerospace Aerodynamics Research Conference, Cambridge, UK (2002) 373-386.